Journal of Atmospheric and Terrestrial Physics, Vol. 46, No. 6/7, pp. 473–488, 1984.
Printed in Great Britain.

0021-9169/84 $3.00 + .00
Pergamon Press Ltd.

Field-perpendicular and field-aligned plasma flows observed by EISCAT during a prolonged period of northward IMF

A. D. FARMER, M. LOCKWOOD, R. B. HORNE, B. J. I. BROMAGE and K. S. C. FREEMAN
Rutherford Appleton Laboratory, Chilton, Didcot, Oxon OX11 0QX, U.K.

(Received for publication 21 February 1984)

Abstract—The effect of a prolonged period of strongly northward Interplanetary Magnetic Field (IMF) on the high-latitude F-region is studied using data from the EISCAT Common Programme Zero mode of operation on 11–12 August 1982. The analysis of the raw autocorrelation functions is kept to the directly derived parameters N_e, T_e, T_i and velocity, and limits are defined for the errors introduced by assumptions about ion composition and by changes in the transmitted power and system constant. Simple data-cleaning criteria are employed to eliminate problems due to coherent signals and large background noise levels. The observed variations in plasma densities, temperatures and velocities are interpreted in terms of supporting data from ISEE-3 and local riometers and magnetometers. Both field-aligned and field-perpendicular plasma flows at Tromsø showed effects of the northward IMF: convection was slow and irregular and field-aligned flow profiles were characteristic of steady-state polar wind outflow with flux of order 10^{12} m^{-2} s^{-1}. This period followed a strongly southward IMF which had triggered a substorm. The substorm gave enhanced convection, with a swing to equatorward flow and large (5×10^{12} m^{-2} s^{-1}), steady-state field-aligned fluxes, leading to the possibility of O^+ escape into the magnetosphere. The apparent influence of the IMF over both field-perpendicular and field-aligned flows is explained in terms of the cross-cap potential difference and the location of the auroral oval.

1. INTRODUCTION

Field-perpendicular convective motions of plasma in the high-latitude ionosphere are known to be driven by the interaction of the magnetosphere with the solar wind and the Interplanetary Magnetic Field (IMF) embedded in it. Two separate mechanisms have been proposed—magnetic merging of the IMF with the geomagnetic field, and a viscous-like interaction at the magnetopause. The viscous interaction is independent of the direction of the IMF, while the merging mechanism gives two-celled convection with antisolar flow along the day–night separatrix when B_z is negative (southwards), and sunwards flow with a shrunken convection pattern when it is northwards. For B_z negative, field-line merging occurs at the low-latitude magnetopause, and for B_z positive, at the poleward edges of the cusps, though for small positive B_z, the sign of B_y (the component antiparallel to the Earth's orbital track) may determine which occurs.

Sunward convection for northward IMF has since been confirmed by various satellite ion-drift experiments (e.g. BURKE *et al.*, 1979), but unlike what one would expect if merging were the only mechanism, the cross-cap potential difference, Φ, does not go to zero when the IMF is northward. It has a residual value of about 35 kV (REIFF *et al.*, 1981) because, although the central polar region driven by the merging mechanism has sunward flow, there is a viscously-driven flow around it (giving a four-celled pattern) which dominates in terms of total cross-cap potential. Hence the major part of the large Φ (up to about 150 kV) observed when the IMF is southward is due to low-latitude field-line merging, but there is also some contribution from a viscous-like interaction which persists when the IMF is northward.

BURKE *et al.* (1979) found that if B_z exceeded 0.7 nT in their database of S3-2 observations, the pattern was never of two simple cells, but was either four-celled or highly irregular. (Below 0.7 nT the B_y component can maintain the two-cell pattern.) MAEZAWA (1976) and HORWITZ and AKASOFU (1979) set the limit for maintenance of a two-cell pattern at 1 nT. The *irregularity* of the pattern becomes more marked during long periods of low magnetic activity (HEELIS and HANSON, 1980; OLIVER *et al.*, 1983) and in winter (BURKE *et al.*, 1979).

Field-aligned plasma motions at low altitudes (below the $F2$ peak) are dominated by the effects of thermospheric winds through ion–neutral collisions. Solar heating by EUV and UV radiations drives winds across the polar cap, roughly parallel to the 1300–0100 local time axis. At high latitudes considerable deviations from this simple wind pattern are caused by convection electric fields, which are sources of energy and momentum, via Joule heating and ion drag, respectively. Observations and models show that for the latitude of EISCAT, the meridional wind component is mainly poleward by day and equatorward at night (REES *et al.*, 1980), giving, respectively, lowering and raising of the F-layer (RISHBETH, 1977). The ion–neutral collision frequency decreases with altitude and plasma diffusion becomes the dominant process in determining field-aligned flow in the topside. The height profiles for O^+ production and loss cause downward flow at all altitudes just above the $F2$ peak in diffusive equilibrium. At greater heights the flow is expected to be upward at the latitude of EISCAT to support the outflow of light ions in the polar wind, which is found to persist along all field lines (open or closed) outside the outer plasmasphere (TITHERIDGE, 1976; HOFFMAN and DODSON, 1980). At altitudes where the photochemical reaction rates (production and loss) and the densities of other ion species (molecular and light ions) are negligible, the O^+ flux will equal the total ion outflow under steady-state conditions. However, time-dependent filling or depletion of the topside ionosphere will cause differences between these two flux values (WHITTEKER, 1977). In the classical, steady-state theory of thermal polar wind escape, the total ion flux is predicted to be 10^{12} m^{-2} s^{-1} (and almost entirely light ions), supported, via charge exchange, by an upward O^+ flow of equal magnitude at lower altitudes (BANKS and HOLZER, 1969). Mean light ion flows of this value were found at 1400 km and high latitudes for $Kp < 2$o by HOFFMAN and DODSON (1980), on the assumption that the dominant O^+ ions are stationary. This agrees with the mean field-aligned O^+ flow near 500 km inferred by LOCKWOOD (1982, 1983) for $Kp < 3$o from a large number of topside soundings (about 1000). If the instantaneous O^+ and H^+ flows at different altitudes along the same field line were equal to these mean values, the flow would be a steady-state polar wind, as predicted by BANKS and HOLZER (1969). Hence, in an average sense, these two studies together imply such a polar wind at low Kp. Larger mean O^+ flows (up to 10^{13} m^{-2} s^{-1}) were found at all polar latitudes for greater Kp, and in localised regions ($< 5°$ in latitudinal extent) in the auroral oval for low Kp. Such flows could be due to enhanced steady-state flows into the magnetosphere or to transient refilling of the topside ionosphere. The IMF is expected to affect the field-aligned flow at a given latitude primarily through the level of geomagnetic activity and motions of the auroral oval.

The auroral oval is known to move to very high latitudes during prolonged periods of northward IMF (AKASOFU et al., 1973). The equatorward edge of the electron precipitation lies on the same L-shell as the inner edge of the plasma sheet, i.e. on the boundary between co-rotating and convecting plasma. The invariant latitude of the equatorward precipitation boundary, Λ_B, will therefore depend on the cross-tail, dawn-to-dusk electric field (KIVELSON and SOUTHWOOD, 1975), and hence on the IMF. From ISIS particle observations KAMIDE and WINNINGHAM (1977) found Λ_B to be positively correlated with hourly means of B_z with a 1 h lag. HARDY et al. (1981), however, noted from a larger database of DMSP-$F2$ particle data that, for the local times studied, the correlation was only valid for $B_z < 1$ nT. For strongly northward IMF ($B_z > 1$ nT) they found little correlation or slight anticorrelation. From the same data, GUSSENHOVEN et al. (1981) found a positive correlation with the current Kp value, throughout the range of Kp. Both ISIS and DMSP-$F2$ show that the low-latitude boundary of electron precipitation will, on average, lie very close to the Tromsø field-line at local midnight, if the IMF is northward. However, the scatter in these data is large, such that EISCAT may or may not remain within the precipitation oval under these conditions.

2. EISCAT OBSERVATIONS AND DATA ANALYSIS

The Common Programme Zero (CP0) mode of operation was employed on the EISCAT facility between 1000 UT on 11 August 1982 and 1000 UT the following day. In this mode the azimuth and elevation of the Tromsø antenna are fixed so as to give approximate magnetic field-alignment of the radar beam at 300 km. A total of 23 overlapping scattering volumes, each spanning 54 km in range and separated by 27 km, are selected by the gating of the Tromsø receiver. This produces an altitude coverage, for the centre of the scattering volumes, of 128–705 km. The pointing directions of the Kiruna and Sodankylä antennae intersect the Tromsø beam near 300 km. The bulk plasma velocities, obtained from the Doppler shifts of the signals received at the three sites, can be resolved into a field-aligned and two orthogonal field-perpendicular components at this height. In this paper these are defined with respect to the local magnetic field line at Tromsø as given by the IGRF80 definitive magnetic field model, with $v_{\perp N}$ being positive in the magnetic north direction, $v_{\perp E}$ positive magnetically eastwards and $v_{\parallel}$ taken as positive parallel to the magnetic field, i.e. downwards.

The autocorrelation functions (acfs) recorded at all three sites have been post-integrated in 5 min intervals and, after subtraction of the average of the four furthest background noise gates, fitted to give the plasma density, N_e, the velocity along the Tromsø beam, v_T, the electron temperature, T_e, and the ion temperature, T_i. The analysis program used assumes a fixed ion composition profile, with only O^+ ions above 220 km and O^+ and a mixture of molecular ions (of mean mass

30.5 a.m.u.) at lower altitudes. The proportion of O^+ ions was taken to rise from 19% at 128 km to 100% at 220 km.

The assumption of negligible light ion concentrations is valid for the height range studied. TITHERIDGE (1976) found that under polar wind outflow conditions, such as prevail at the latitude of EISCAT, the ion transition height (where O^+ and H^+ densities are equal) is large at all local times, varying between 900 and 1200 km in winter and 1100 and 1200 km in summer. Ion mass spectrometer results from the ISIS-2 satellite reveal that, on average, O^+ is an order of magnitude more abundant at 1400 km than the major light ion, H^+, at these latitudes during summer and equinox and by a smaller factor during winter (HOFFMAN and DODSON, 1980). In this paper no altitudes greater than 650 km are considered, owing to the low signal-to-noise ratio of echoes received from above this height. Hence light ions can be neglected.

The errors introduced by the assumed profile for the fraction of molecular ions are harder to assess. SOJKA *et al.* (1982) predict that for strong convection significant densities of O_2^+, NO^+ and N_2^+ should exist at some local times at the latitude of EISCAT, notably in the mid-latitude trough during winter and in the afternoon sector during summer. ISIS-2 measurements have revealed large molecular ion fractions at 1400 km for high latitudes during major geomagnetic storms (HOFFMAN *et al.*, 1974). To estimate the effects of such enhancements of molecular ion density, synthetic, noise-free acfs have been generated and then fitted using the data analysis procedure employed for this paper, with various assumed ion compositions. Errors in the geophysical parameters introduced by the assumed composition were then evaluated by comparing the analysis program outputs (N_e', T_e', T_i') with the values used to synthesise the acfs (N_e, T_e, T_i). Figure 1 shows the errors in N_e', T_e' and T_i' as a function of assumed percentage of O^- in a mixture with molecular ions of mass 30.5 a.m.u. All ion species have a temperature of T_i and a bulk velocity v_i, giving no error in the computed velocity ($v_i' = v_i$). The curves are for $N_e = 10^{11}\ m^{-3}$, $T_e = T_i = 1000$ K and (a) 50% O^+ ions (50% molecular ions) and (b) 70% O^+ (30% molecular). For these two cases N_e is accurate to within 12%. The largest error is an overestimate and arises for case (a), when the molecular ion population is entirely neglected by the analysis program. This case also gives maximum overestimates for T_e and T_i (34% and 20%, respectively). However, the temperature errors are larger still if the assumed molecular ion fraction is too large. Then T_e and T_i are underestimated by up to 50%. We conclude that, although errors are not likely to be as large as these worst-case maxima, observed electron and ion temperatures at low altitudes (< 300 km) must be treated with particular caution.

Noise of a known temperature was injected into the receiver system and recorded in a calibration gate. In the analysis of acfs, this was used to calibrate received power to allow for the gain variations of the receiver system (excluding antenna). The transmitted power was assumed to be 1 MW, the approximate power being

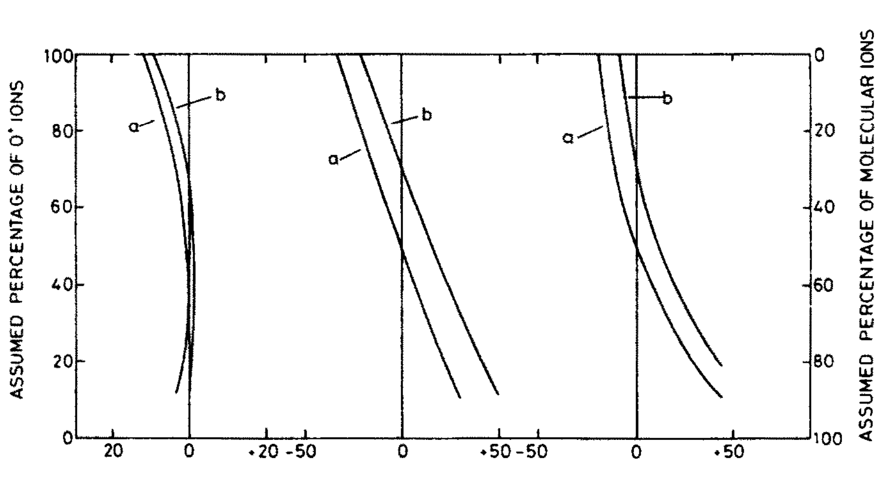

Fig. 1. Percentage errors in observed electron density, electron temperature and ion temperature (N_e', T_e' and T_i') from their true values ($N_e = 10^{11}\ m^{-3}$, $T_e = 1000$ K and $T_i = 1000$ K) as a function of assumed percentages of O^+ and molecular ions, mean mass 30.5, with a true ion composition of (a) 50% O^+, 50% molecular ions and (b) 70% O^+, 30% molecular ions.

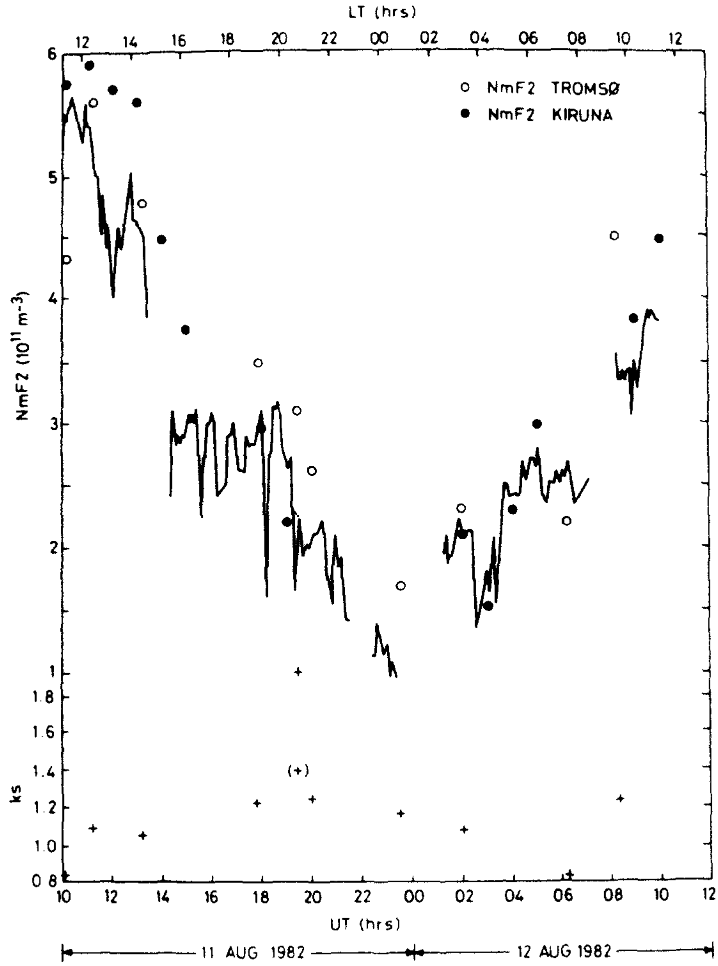

Fig. 2. Peak density of the $F2$ layer observed by EISCAT (solid line), Tromsø ionosonde (open circles) and the Kiruna ionosonde (closed circles) on 11–12 August 1982. Crosses give the system factor estimates, k_s, defined as the $NmF2$ value from the Tromsø ionosonde divided by that from EISCAT.

transmitted at this time. Deviations from this value would have caused a change in the system factor, defined here as the ratio of the true peak density, $NmF2$, to the value determined by EISCAT.

Figure 2 shows the $NmF2$ values determined from the EISCAT observations during the 24 h CP0 run. The solid and open circles are the values of $NmF2$ scaled from the ordinary-wave traces of ionograms recorded at Kiruna and Tromsø, respectively. The crosses give the estimate of the system factor, k_s, obtained using the Tromsø ionosonde values for $NmF2$. The forms of the variations of the three $NmF2$ estimates were similar. However, k_s varied between 0.8 and 1.9. The largest k_s value was for an EISCAT 5 min post-integration, for which $NmF2$ was much smaller than for adjacent ones. Extrapolation of the adjacent values (dotted line) would reduce this k_s estimate to 1.4 (shown in parentheses).

This still leaves a large and gradual variation in k_s. One major cause may be off-vertical reflections of the ionosonde trace, which could cause the ionosonde to measure $NmF2$ for a location that is a considerable distance from the Tromsø beam. Such effects are expected when the spatial variations of the $F2$-layer are large (NYGREN, 1977). At 1100 UT on the 11th and 0200 UT on the 12th the $NmF2$ values observed by the Tromsø and Kiruna ionsondes were approximately equal, implying a nearly horizontally stratified F-region. These values were also close to the EISCAT value at these times, giving k_s of 1.1 in both cases. The implied lack of spatial structure makes these two k_s values the best available estimates of the true system factor. However, bearing in mind the large range of other k_s values, we have elected not to multiply by any ionosonde-derived system factors in this paper to give absolute N_e values. Hence, when discussing ion density or flux, the reader should bear in mind that they could be multiplied by a system factor, for which we believe the most reliable estimate is 1.1 at all times. Note, also, that some real variation in the true system factor may still have occurred, due to changes in transmitter power, noise injection level or receiver gain.

Examples of results from the analysis are shown in Fig. 3, which plots T_e in the vertical direction, with time running up the diagram to the right and altitude up and to the left. The value of T_e has been set to zero during data gaps, which have a variety of causes: changing data tapes, system faults, failure of the analysis to converge on a fit, and so on. In general T_e increased uniformly with altitude and changed smoothly with time at the lower altitudes, but displayed random fluctuations, with both time and altitude, for the furthest ranges. The ion velocity data showed similar (but considerably larger) fluctuations in the furthest range gates, whereas they are almost completely absent from the electron density data. The amplitude of these fluctuations increased rapidly if the signal fell below 0.2 of the background noise (SNR < 0.2). Experiments using different frequencies to observe the same scattering volume (the U.K. Special Programme 'Polar' or EP111) have been analysed and revealed this effect in all frequency channels. In addition, the various frequencies gave different results, the differences also increasing rapidly as SNR falls (BROMAGE, 1984). In this paper we have only considered data for which SNR exceeds 0.2. The observed SNR values are shown in Fig. 4, using the same form of data presentation as Fig. 3 but with the height axis reversed so the distribution is viewed from the topside. The solid line marks the SNR = 0.2 level, and this varied between 350 km and 500 km in height.

Figure 5 shows the variances of the analysis fits to the 5 min post-integrated raw data. In general the fit was poorer (larger variance) for the lowest ranges. Comparison with Fig. 4 demonstrates that this was not related to low SNR, but may have been due to the scale heights of ionospheric variations being smaller than the scattering volume, erroneous ion composition assump-

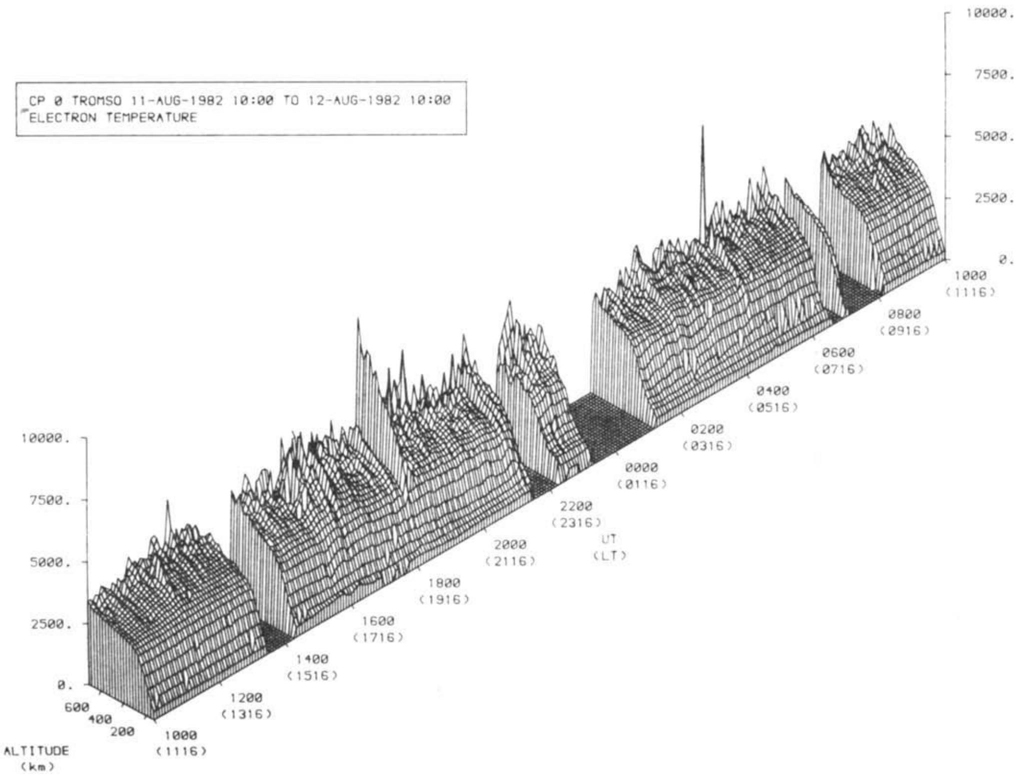

Fig. 3. Electron temperature, T_e, as a function of altitude and Universal Time, viewed from the bottomside. Local times are given in brackets. Results from all fits that converged have been included.

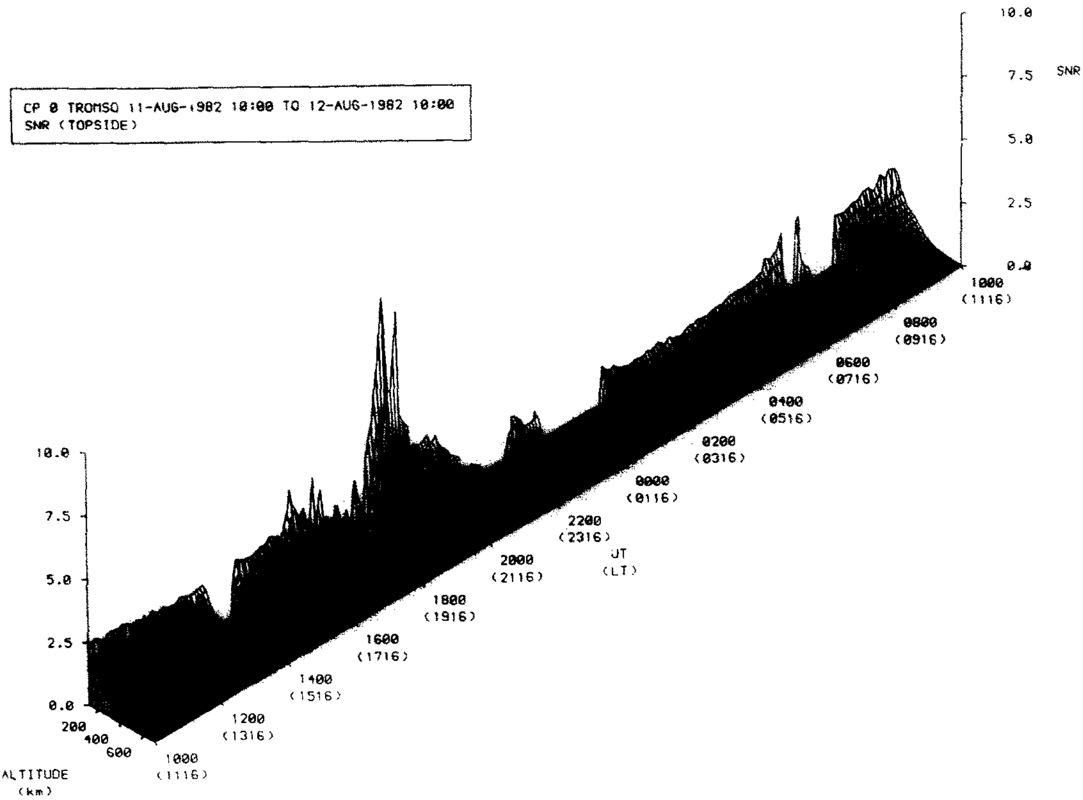

Fig. 4. Signal-to-background noise ratio, SNR, as a function of altitude and Universal Time, viewed from the topside. The solid line is the SNR = 0.2 level.

tions or local oscillator variations in the receiver. In addition, there were some 5 min integrations for which the variance was high at all altitudes. Figure 6 shows the results of detailed examination of the first such feature in Fig. 5, at 1135 UT. A large coherent signal can be seen in background gates 30 and 31, from the spectra, $S(f)$, and the imaginary part of the acfs, $\rho_I(\tau)$. In this example, subtraction of the average of background gates causes considerable distortion of the signal spectra. This coherent signal is probably an echo from a satellite. The fit variances, VAR, for the signal gates, exceeded 25 (arbitrary units), as compared to a maximum of about 5 for adjacent data points. A limit of 15 for the fit variance was chosen in order to eliminate data containing major coherent signal effects. In this paper these gates have simply been discarded, although such data could be cleaned and used by omitting from the post-integration those individual gates that contain any coherent signal.

The two cleaning criteria of SNR > 0.2 and VAR < 15 have been applied to the electron temperatures shown in Fig. 3, and the remaining points plotted in Fig. 7. Values excluded have been put to zero, unless they were between two valid data points, in which case linear interpolation was used in time or, preferably, in altitude. It can be seen that the random fluctuations and anomalous features due to noise have been removed. In subsequent plots the data cleaning procedure described above has been employed.

3. INTERPLANETARY AND GEOMAGNETIC CONDITIONS

Figure 8 shows the Interplanetary Magnetic Field (IMF) and solar wind conditions for this period of CP0 observations. These data were recorded by the ISEE-3 satellite, which at that time was in orbit near the Earth–Sun L1 libration point and about 240 R_E from the Earth. The top panel shows the B_z component of the IMF, defined as positive northward and in the Geocentric Solar Magnetospheric reference frame (RUSSELL, 1971). ISEE-3's distance from the Earth means that it was measuring interplanetary conditions about 0.6–1.0 h before they reached Earth. Because of the distance, one cannot be sure the fine detail seen at

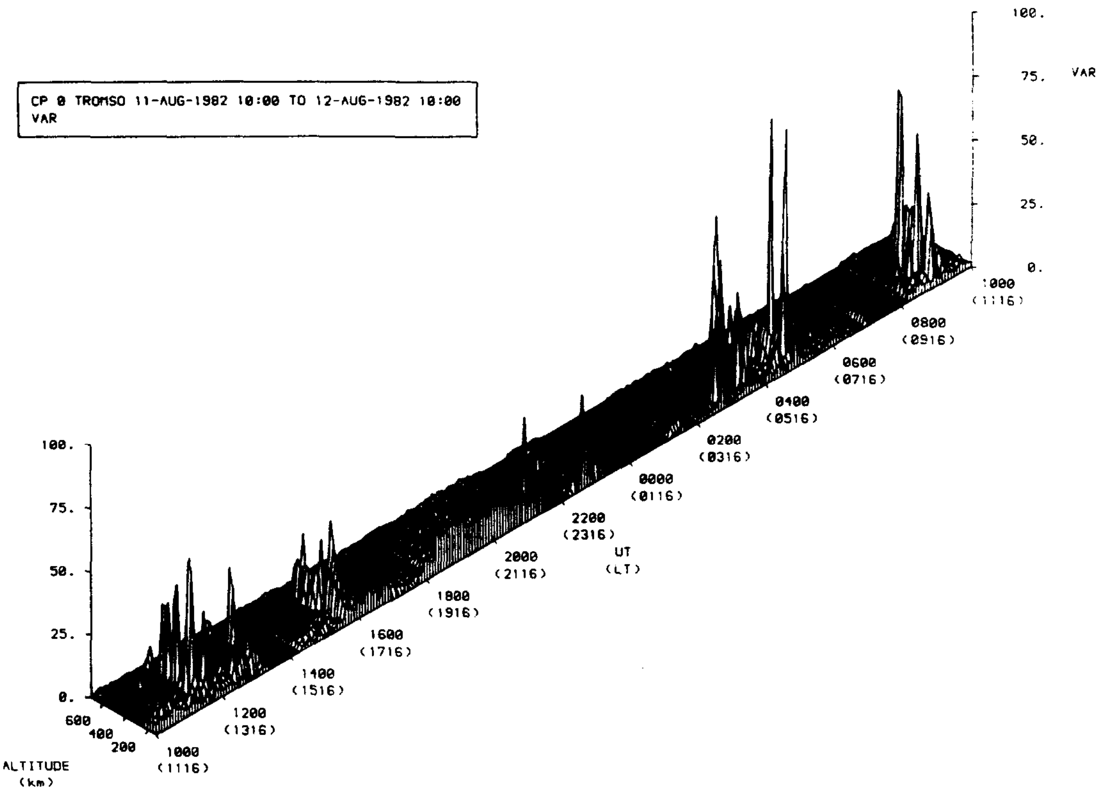

Fig. 5. Variance of analysis fit to raw data, VAR, as a function of altitude and Universal Time, viewed from the bottomside.

the spacecraft will be the same as reaches the Earth, so one should only consider the overall trends as applicable there. The IMF was northward for a large part of the period of observation. In particular, it was strongly and consistently northward between 2100 UT on 11 August and 0400 UT on the 12th. The dashed line in Fig. 8 shows the $B_z = 1$ nT level, below which normal two-celled convection is expected and above which four-celled patterns, with sunward flow in the polar cap, or irregular patterns have been observed (see introduction).

The lower panel of Fig. 8 shows an energy coupling factor, ε (AKASOFU, 1981), defined here without an area factor, l_0^2, i.e. $\varepsilon = VB^2 \sin^4 (\theta/2)$, where V is the solar wind speed, B is the IMF strength and θ is the polar angle of the IMF. As is to be expected, ε was very small throughout the period of predominantly northward IMF, but peaked near 1600 UT when the IMF was strongly southward. This peak value of 6×10^7 nT^2 m s^{-1} corresponds to a value of 1.2×10^{19} ergs s^{-1} for the cgs units and definition adopted by AKASOFU (1981), using his typical value of 7 R_E for l_0.

A summary of geomagnetic and riometer activity during this 24 h, as observed in the vicinity of the Tromsø field line, is given in Fig. 9. The period of predominant strongly northward IMF coincided with low values of the 3 h indices of magnetic activity, both the planetary Kp and the local K for Sodankylä. In addition, the magnetometer traces from Kiruna were quiet during this period and low absorption was recorded at the three Finnish riometer observatories shown in Fig. 9.

The values of ε around 1600 UT are sufficiently large to trigger a magnetic substorm (AKASOFU, 1981) and this was observed in the magnetometer and riometer records. The high level of magnetic activity persisted until 2000 UT, when a second and smaller peak in riometer absorption was observed.

4. EISCAT RESULTS FOR N_e, T_e AND T_i

The electron densities observed along the Tromsø beam are displayed in Fig. 10, viewed from the bottomside. Large enhancements in the lowest range

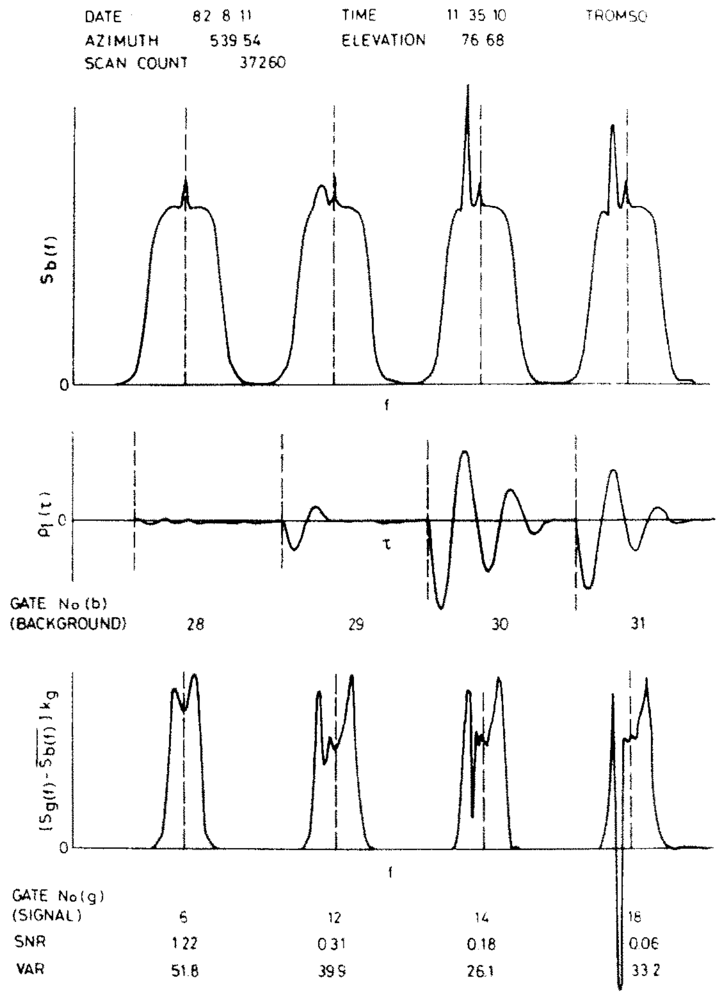

Fig. 6. Spectra, $S(f)$, and imaginary parts of acfs, $\rho_I(\tau)$ (as a function of frequency, f, and correlation time, τ, respectively) for background gates (numbers 28–31) for 1135 : 10 UT. The bottom panel shows signal gate spectra with the average of the background gates subtracted. k_g is a numerical scaling factor for each gate.

gate were observed after 1600 and 1900 UT and coincide with the enhancements in riometer absorption shown in Fig. 9, and were therefore probably due to energetic particle precipitation. Note that no such enhancement is seen near 0600 UT on the 12th, when the riometer absorption was again enhanced, implying the precipitation at this time was more energetic or had greater spatial structure.

The overall behaviour of the F-layer is reminiscent of a mid-latitude diurnal variation in that the peak density decayed to about one-sixth of its value at local noon (see Fig. 2). The ionosphere was in direct sunlight at all times, but the photo-ionisation rate is dependent on the solar zenith angle. The density observed at 160 km, where production and loss dominate, varied in a similar manner to $NmF2$, between a maximum of $1.8 \times 10^{11}\ m^{-3}$ and a minimum near local midnight of $4 \times 10^{10}\ m^{-3}$. The model of SOJKA et al. (1982) predicts that for summer solstice, at the latitude of Tromsø and this height, densities will be of the order of $10^{11}\ m^{-3}$ at all local times. The densities near midnight, when photo-ionisation is reduced, are maintained by auroral particle precipitation. If this precipitation were absent, the model predicts that densities would fall to about $3 \times 10^9\ m^{-3}$, due to the solar zenith angle change. Hence, we infer nightside precipitation production at 160 km, but not as great as that included in the SOJKA et al. (1982) model. It is not known if the same is true for greater altitudes (i.e. for softer precipitation), however, the model does not predict the factor-of-six decrease in

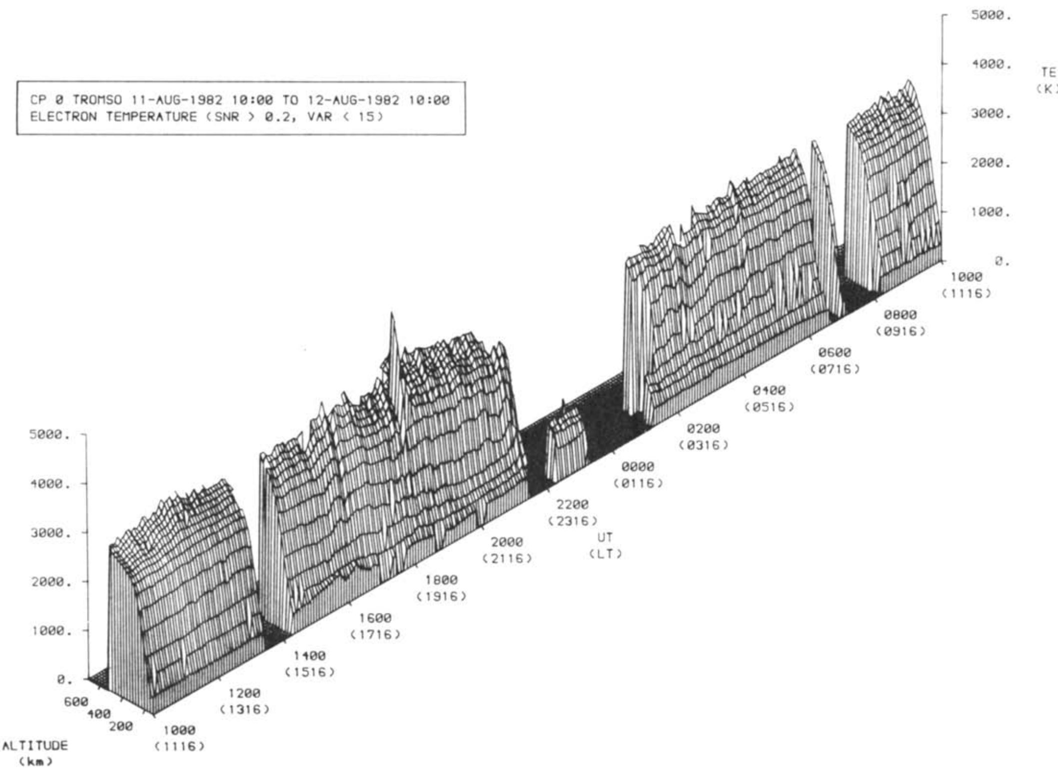

Fig. 7. Electron temperature, T_e, as a factor of altitude and Universal Time, viewed from the bottomside. Only results for which VAR < 15 and SNR > 0.2 have been included.

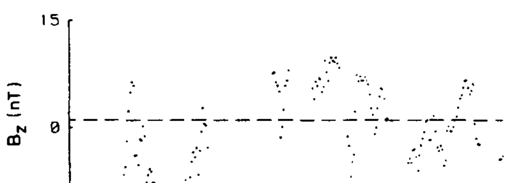

Fig. 8. Northward component of the IMF, B_z, in the geocentric solar ecliptic frame and the ε factor (defined as $B^2 V \sin^4(\theta/2)$, where B is the IMF strength, θ is the polar angle of the IMF and V is the solar wind speed) from ISEE-3 observations for the period of EISCAT CP0 observations on 11–12 August 1982.

densities shown in Figs. 2 and 10. The lowest F-region densities were observed when the IMF was northward (see Fig. 8), but there is no clear indication that this was a causal relationship, only that the gradient with time was steepest about an hour after B_z switched sense (1900 and 0300 UT).

The observed ion temperatures are displayed in Fig. 11 and reveal considerably larger variations than the electron temperature (Fig. 7). The electron temperature was elevated over the ion temperature (T_e/T_i consistently exceeded 1.8 at heights over 400 km) and the T_e gradient remained positive at the greatest heights. These two facts indicate that the electron energy budget was controlled by thermal conduction (i.e. that electron-to-ion energy losses were low, which would be the case for sufficiently low N_e) and that downward heat flow from the magnetosphere was present (BANKS and KOCKARTS, 1973).

Joule heating is known to be particularly intense around the auroral oval in the afternoon sector during summer, due to the combination of large electric fields and high ionospheric conductivity. For moderate magnetic activity (Kp = 3–6) during summer at the

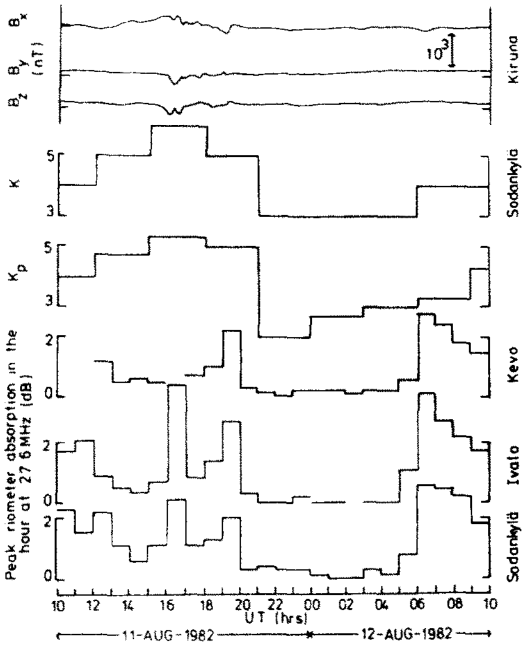

Fig. 9. Local magnetic field at Kiruna, K index values for Sodankyla, Kp, and hourly maxima of riometer absorption observed at Sodankyla, Ivalo and Kevo for the period of EISCAT observations on 11–12 August 1982.

latitude of EISCAT, FOSTER *et al.* (1983) found that, on average, strong Joule heating occurred between 1600 and 2000 local time using 4 years' AE-C data. Joule heating raises the ion temperature at altitudes from the E-region, where the heating occurs, up to heights where the neutral density is so low that T_i is tied to T_e by electron–ion energy exchange (when T_e/T_i tends to unity) (BANKS and KOCKARTS, 1973). The electron temperature, however, is not raised by electric fields, except perhaps in the E-region by plasma waves (SCHLEGEL and ST. MAURICE, 1981). Hence, the ion temperature rise at all heights between 1400 and 1615 UT may have resulted from Joule heating due to the large westward flows (see Fig. 12). Note, however, the sudden fall of T_i at 1615 UT.

The ionosphere was in sunlight at all times and the photo-electron heating rate would have been large. Soft particle precipitation will cause additional T_e rises in the F-region (ROBLE and REES, 1977), but the efficiency of ion heating by this process is less than 5% (STAMNES and REES, 1983). No coincident rises in both T_e and N_e (but not T_i) which could be attributed to particle precipitation can be identified in Figs. 7, 10 and 11.

5. EISCAT RESULTS FOR PLASMA MOTIONS

The pattern of field-perpendicular motions, observed during the 24 h, is plotted in Fig. 12. To the left are all available results for each 5 min post-integration and on the right these have been averaged into groups of four for clarity. Local noon is at the top of each plot. Observations commenced at 1000 UT (A) and until 1200 UT flows were small, slightly irregular, but generally northward into the cap as expected. Between 1200 and 1800 UT the velocity was large and westward, as expected for normal convection at a sub-auroral latitude in the afternoon sector. Until 1500 UT the velocity was slightly poleward. However, near 1600 UT it turned rapidly to equatorward. This could have been due to a temporal change in the flow pattern, caused by the moderate substorm at 1600 UT. Previous observations show that substorms tend not to affect the convection pattern other than to produce a general expansion and an increase in plasma speeds (see references given in LOCKWOOD *et al.*, this issue). The southward turning of the flow implies that the polar cap boundary was approaching Tromsø and the convection pattern was of a type commonly observed by the AE-C ion drift experiment (see Fig. 11c of HEELIS and HANSON, 1980). For this type of pattern the polar cap boundary is an equipotential extending further into the night-side around dawn than around dusk, giving shear flow reversals at the cap boundary in the afternoon sector, which turn to rotational reversals as the cap boundary potential begins to increase. In order to explain the onset of large southward flow near 1600 UT, this transition must occur at a local time near 1800, depending on how far north of Tromsø the cap boundary lies. The strong dusk convection cell was observed when the IMF was strongly southward and hence the cross-cap potential difference, Φ, was large (see Fig. 8). Figure 4a of REIFF *et al.* (1981) plots Φ as a function of ε (unmodified by their allowance for solar wind compression at the magnetopause) and interpolation of these AE-C data gives a value for Φ of about 100 kV, corresponding to the peak ε of 6×10^7 nT^2 m s^{-1} shown in Fig. 8. This is a large driving potential and convection should therefore have been strong at this time.

The B_z component of the IMF increased to over 1 nT at some time during the ISEE-3 data gap between 1800 UT and 2100 UT. The data prior to 1800 UT suggest that this occurred close to 1800 (Fig. 8). Figure 12 shows that the convection velocities were highly irregular when $B_z > 1$ nT (until 0400 UT). Large flows (consistently eastward but highly variable in the north–south direction) were seen for about an hour after local midnight. Unfortunately, this is another period for

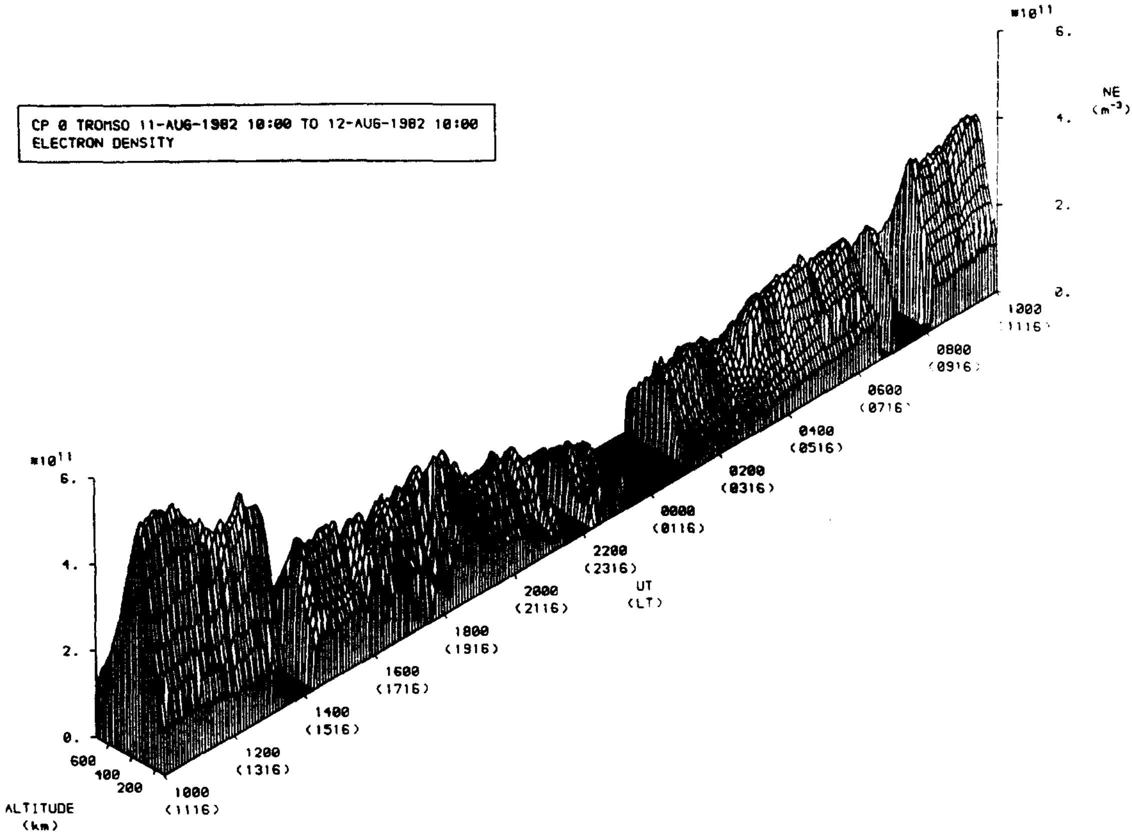

Fig. 10. Electron density, N_e, as a function of altitude and Universal Time, viewed from the bottomside.

which ISEE-3 data are missing, hence, it is not known if a southward excursion of the IMF occurred at this time. The brief excursions which were observed were accompanied by a short period (usually a single 5 min post-integration period) of larger velocities. More regular eastward convection was observed in the available EISCAT data when the IMF returned to southward (0600–0700 UT).

The field-perpendicular velocities, $v_{\perp N}$ and $v_{\perp E}$, are plotted separately in Fig. 13 for the height of intersection of the beams (298 km). Also shown are the field-aligned component, $v_{\parallel}$ (positive values downward), the height of the $F2$ peak and T_e and T_i for a height of 443 km. It can be seen that the rapid southward flows observed just after 1600 UT coincided with a sudden decrease in $hmF2$ of about 75 km. Such a southward velocity will have a downward component due to the inclination of the magnetic field line and, hence, the westward electric field also causes electrodynamic lowering of the F-layer (RISHBETH, 1977; SCHUNK and RAITT, 1980). The westward velocities in the afternoon sector increased until 1500 UT and then the southward flows increased until 1600. This period is marked by a gradual rise in T_i, which may in part have been due to *in situ* Joule heating. Throughout this period, $v_{\parallel}$ was downward (see later). The southward motion between 1500 and 1615 was accompanied by a decrease in F-region densities, consistent with the electrodynamic lowering of the plasma to regions of enhanced loss (SCHUNK and RAITT, 1980). However, at 1615 UT, N_e began to rise again and $v_{\parallel}$ turned sharply to upward. The delay between plasma leaving the auroral oval and reaching the Tromsø field line, t_d, will have fallen between 1500 and 1615 for three reasons: firstly, the local time variation of the latitude of the oval; secondly, the observed increase in southward flow; thirdly, expansion of the oval, with the observed increase in magnetic activity. The fact that N_e started to increase at the same time that plasma began to stream up the field line implies that soft precipitation had commenced at Tromsø for the last of these three reasons. Numerical, time-dependent models of the response of the ionosphere to precipitation show that N_e enhancements die away

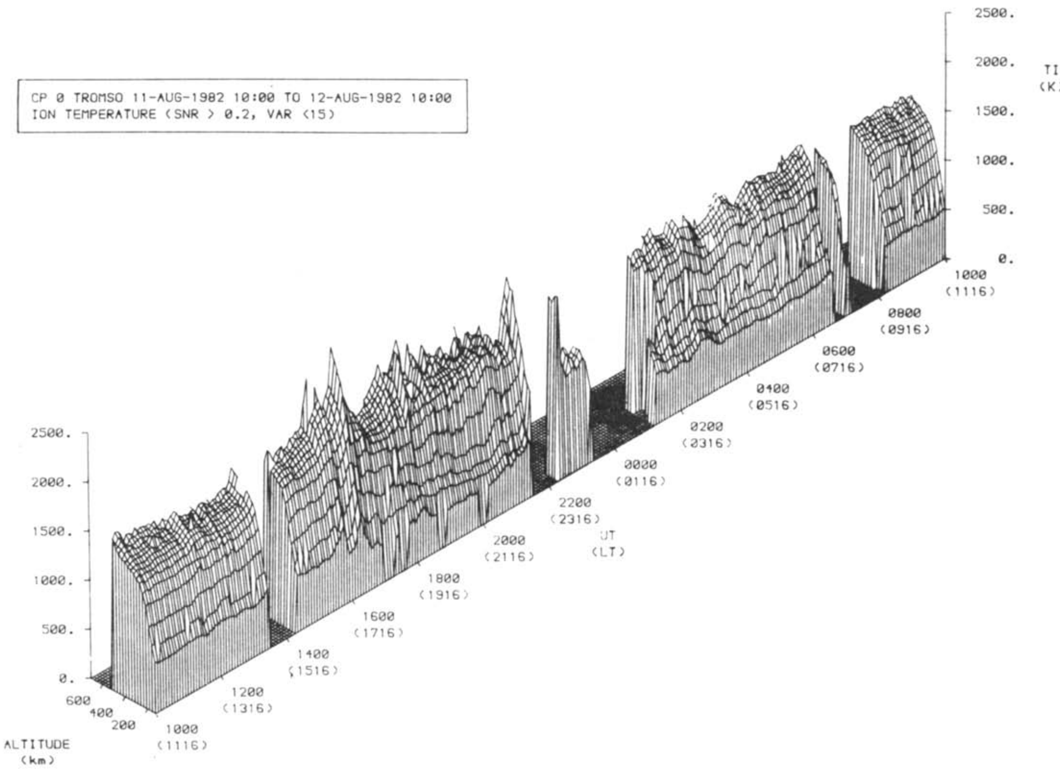

Fig. 11. Ion temperature, T_i, as a function of altitude and Universal Time, viewed from the bottomside.

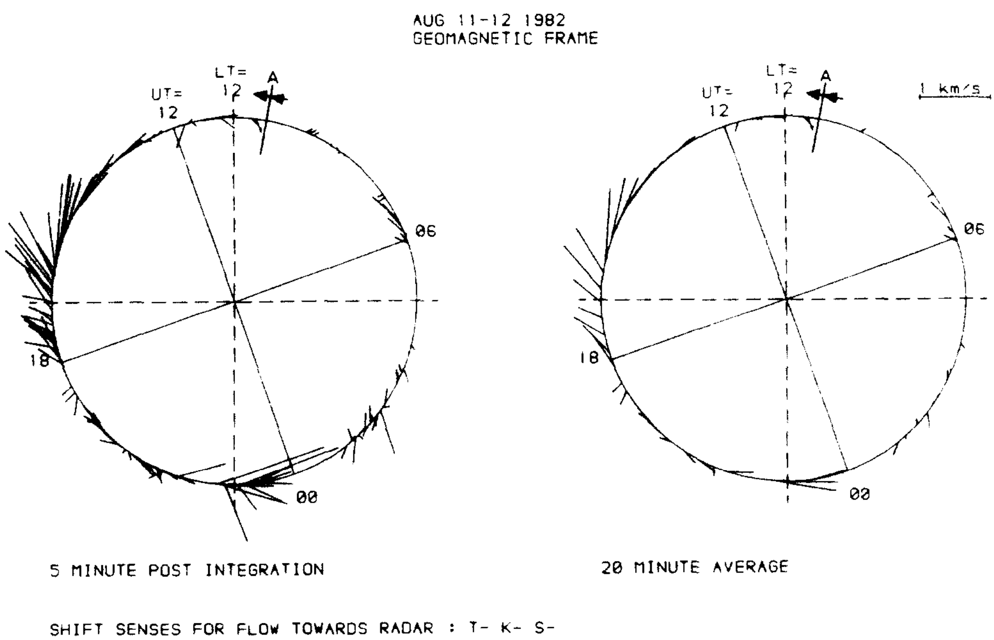

Fig. 12. Polar plot of field-perpendicular velocities. Each vector is plotted with $v_{\perp N}$ radially inwards and $v_{\perp E}$ tangentially anti-clockwise, and points away from the circular locus of the intersection scattering volume. A scale for the vectors is given in the top right and A denotes the start and end time of the 24 h observation run.

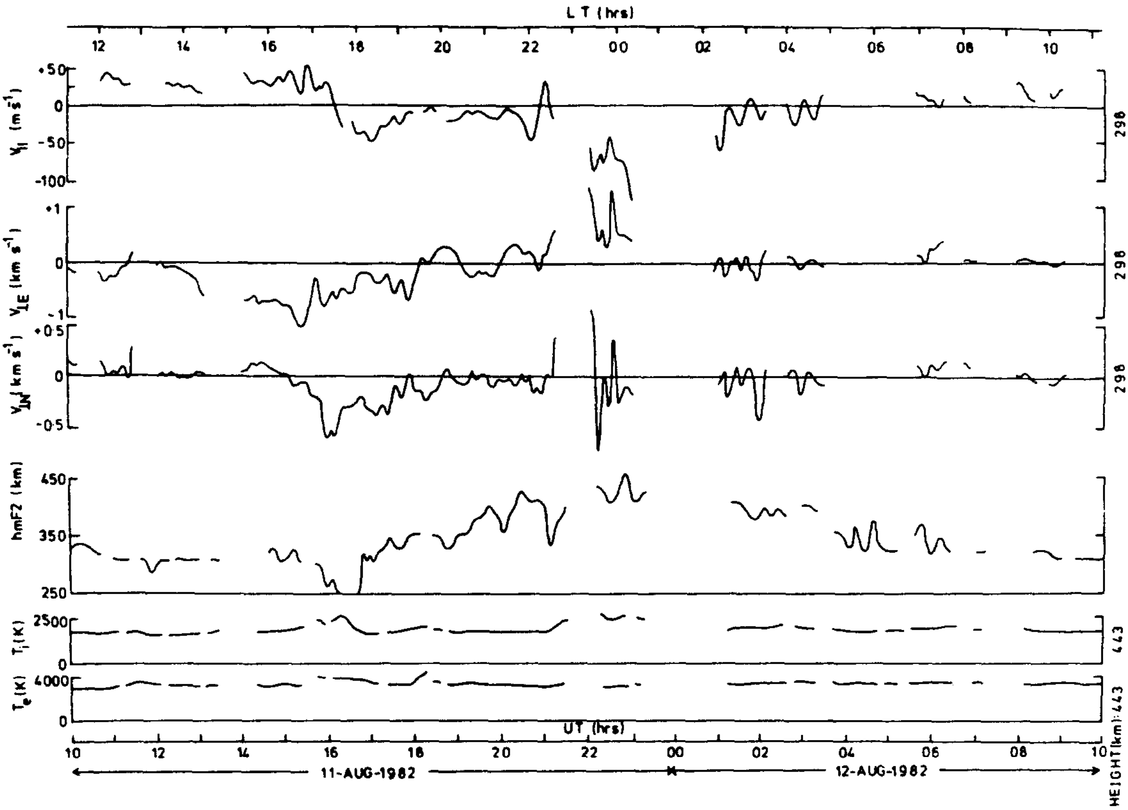

Fig. 13. Observed velocity components, $v_{\perp N}$, $v_{\perp E}$ and $v_{\parallel}$, at altitude 298 km, the $F2$ peak height, $hmF2$ and T_e and T_i at 443 km observed for 11–12 August 1982.

with increasing positive t_d. However, $v_{\parallel}$ is downward below about 1000 km for $t_d > 0$ and is only expected to be upward while precipitation persists (Whitteker, 1977).

The shift to upward flow near 1615 UT was seen at all altitudes. Figure 14 shows the plasma flux along the Tromsø beam, $N_e v_T$, where v_T is defined by the radar convention, i.e. positive values are downward flows. The divergence of the Tromsø beam from the magnetic field line was such that deviations of v_T from $v_{\parallel}$, due to the field-perpendicular motions, will be smaller at 500 km than at 300 km. Large upward flows were present between 1600 and 1800, but smaller upflow persisted at all altitudes until 2300 UT. Between 0100 and 0400 UT on the 12th there was quasi-diffusive equilibrium at all heights, and between 0400 and 1000 UT downward flow. Note the anomalous behaviour in the lowest range gate (128 km) in that the sense of flow was often reversed compared to that for 180 km. It is suspected that this was caused by a receiver oscillator problem.

In order to understand these flows, altitude profiles of $N_e v_T$ have been plotted in Fig. 15. The post-integration period of these data has been increased to 30 min to smooth the profiles and extend them to greater altitudes. Eight profiles are shown to demonstrate the behaviour over the 24 h, although they are not all spaced exactly 3 h apart because of the periods of missing data. In the 1000–1030 UT period, thermospheric winds blew poleward, lowering the bottomside F-region plasma and giving positive v_T. Peak $N_e v_T$ occurred near the $F2$ peak height of 325 km (Fig. 13). In the topside, the field-aligned flows are governed by diffusion and were downward at this time, as expected for equilibrium conditions. The magnitude of this downward diffusion decreased with altitude and extrapolation gives a rough estimate of 700 km for the expected transition to upward flow. Subsequently, the neutral wind effect at lower heights decreased, as did the altitude of transition to upward flow (caused by reduced production at great heights). When upward flow was established at all altitudes, quasi steady-state fluxes were observed ($N_e v_T$ is independent of height, neglecting the small divergence of field lines over this

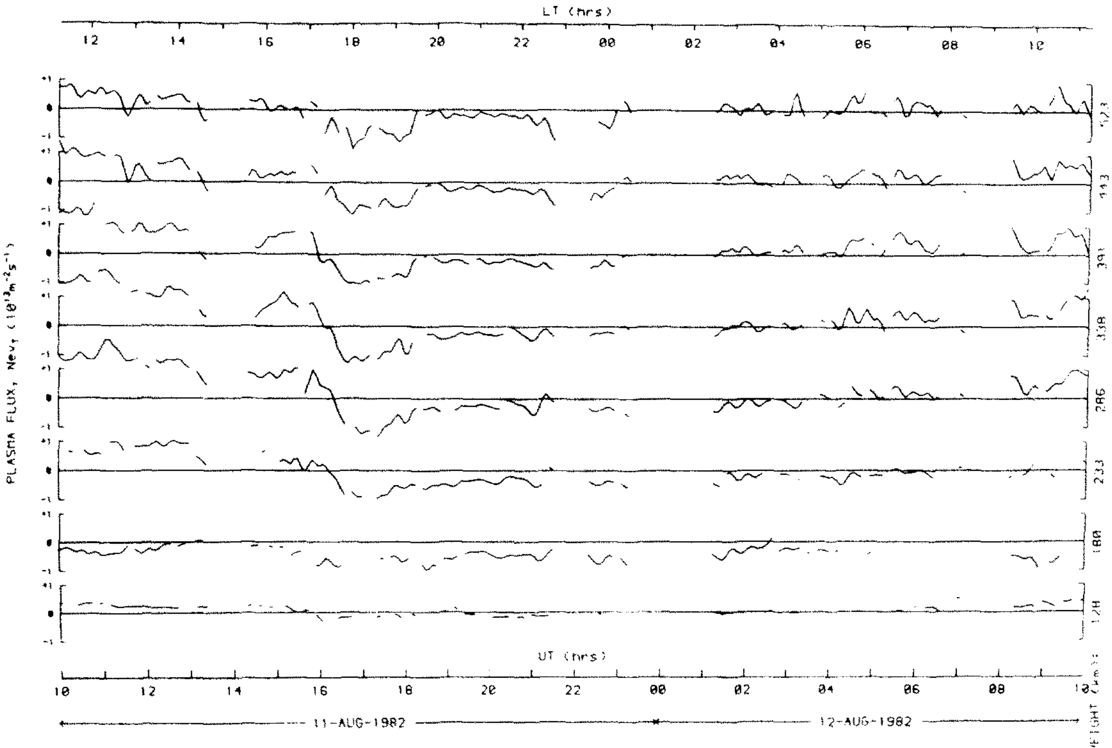

Fig. 14. Plasma flux along the Tromsø beam, $N_e v_T$, at various heights; positive values are downward. The data for 128 km are unreliable.

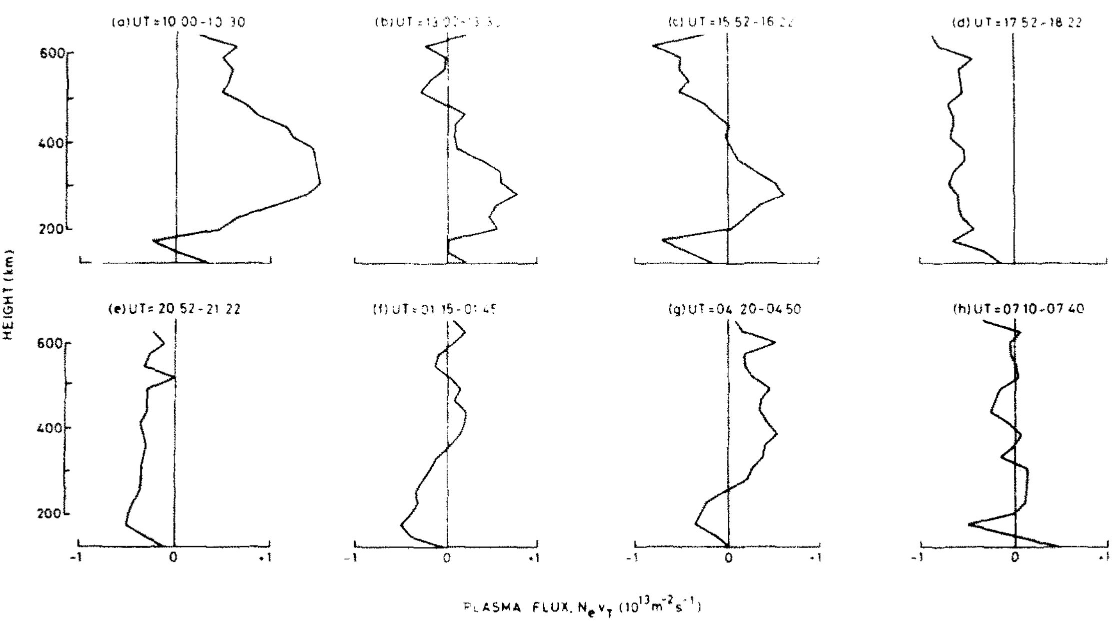

Fig. 15. Altitude profiles of plasma flux along the Tromsø beam, $N_e v_T$, for 30 min integrations of data over 8 time periods.

height range). The mean flux value for altitudes above 400 km was initially over 5×10^{12} m^{-2} s^{-1} at 1800 UT, falling to 10^{12} m^{-2} s^{-1} by 2200 UT. After 0000 UT, the effect of equatorward thermospheric winds could clearly be seen, with upward flows at low altitudes but no clear flow at greater heights. This lifting of plasma by winds had ceased by 0700 UT, when no consistent flow was seen at any altitude. Following this, flows of the type seen at the start of the run were re-established, with plasma below the $F2$ peak being pushed down field lines by thermospheric winds and with plasma drifting downwards at greater heights.

Figure 14 shows that the fluxes turned upward near 1600 UT at 523 km, and at 1615 UT at 233 km. This could have been a response to an ion temperature rise resulting from diffusive equilibrium (Fig. 13), as the plasma was re-distributed according to the increased scale height. However, no equivalent collapse was seen when T_i fell after 1615 UT, and no scale height change is observed. The scale height increase is expected to be less than predicted for a Joule heating rise in T_i, due to electric stress effects (SCHUNK *et al.*, 1975). The change to upward flows must have been a response to precipitation production and heating during the substorm. Figure 14 shows that near 500 km, flows were over 5×10^{12} m^{-2} s^{-1} between 1630 and 1830 UT, indicating major refilling of the topside ionosphere above 500 km or ion escape into the magnetosphere with flux greater than the 10^{12} m^{-2} s^{-1} predicted for the classical polar wind. Similar effects have been reported by LOCKWOOD and TITHERIDGE (1981) and LOCKWOOD (1982) for auroral O^+ flows inferred from topside soundings. As the limitation on light ion outflows (set by charge exchange and Coulomb drag with O^+) is not expected to vary by such a large factor, this implies that O^+ ions were escaping into the magnetosphere. After 1830 UT the flux near 500 km was of the order 10^{12} m^{-2} s^{-1}, consistent with steady-state light ion outflow (HOFFMAN and DODSON, 1980). This situation persisted until the data gap starting at 2300 UT; by the end of the gap at 0100 UT, flows are closer to diffusive equilibrium. During this period, Kp is less than 3, and for these conditions LOCKWOOD (1982, 1983) also found the mean O^+ flux to be 10^{12} m^{-2} s^{-1}. The onset of apparently steady-state outflow at 1839 UT coincided with the cessation of magnetic activity at Kiruna (Fig. 9), following the extrapolated northward turning of the IMF (Fig. 8). HARDY *et al.* (1981) found that the correlation between the equatorward oval boundary, Λ_B, and the IMF B_z component was highest at 1 h lags, for hourly averages of B_z. The upward flow decreased at 1830 UT and, from Fig. 8, the hourly mean of B_z, lagged by 1 h, was -1.5 nT, for which Hardy *et al.* (1981) found a Λ_B of 60–70° at this local time. Hence, it is quite possible that the Tromsø beam ($\Lambda_T = 66°$) was subject to precipitation before 1830 ($\Lambda_T > \Lambda_B$), but not at subsequent times ($\Lambda_T < \Lambda_B$).

Cessation of precipitation caused by a poleward motion of the oval boundary (due to a northward turning of the IMF) would also have caused a decay in N_e. Figures 2 and 10 show that N_e did fall steeply at all heights below the $F2$ peak after 1800 UT. In the topside ionosphere a more gradual decrease in density began at this time. Ionosonde data confirm this decay in N_e (Fig. 2). At all heights the density is lowest while the IMF is northward. In the E-region and lower F-region, this would be expected if a reduction or cessation in precipitation were caused by the poleward motion of the oval. At greater heights, a major plasma source is removed for the midnight sector if plasma is not convected rapidly over the polar cap from the day-side. Hence, the shrunken, four-celled or irregular convection patterns expected when $B_z > 1$ nT do not allow the day-side and cleft regions to act as sources of plasma for the night-side.

6. CONCLUSIONS

Simple criteria for cleaning EISCAT Common Programme 0 data are sufficient to remove most coherent echo and background noise problems and readily allow the dynamical behaviour of the high-latitude ionosphere to be studied. Useful supporting information on the overall morphology of plasma density and temperatures can be obtained from fits to the raw data which assume a model composition profile. However, results must be considered in light of possible errors due to system factor and ion composition changes.

The prolonged northward IMF observed by ISEE-3 during 11–12 August 1982 is found to have had a considerable influence on plasma motions as observed by EISCAT.

As expected from the dependence of the cross-cap potential difference on the IMF, the normal two-celled convection pattern disappeared at $\Lambda = 66°$ when the IMF was strongly and consistently northward. Only small and irregular flows were observed during this period, except when the electron density was at its lowest near local midnight; then some irregular flows of greater speed were briefly observed with no clear correlations with brief southward excursions of the IMF. Prior to this period, a strongly southward IMF triggered a small substorm, causing a southward swing in convection at $\Lambda = 66°$ as the polar cap expanded, with a consequent depression of the $F2$ peak by electrodynamic lowering.

These changes in the IMF coincided with changes in the field-aligned flow as observed by EISCAT. The influence of the IMF on such flows would be indirect, and seemingly via the location of auroral precipitation. When the IMF was northward, agreement with numerical models suggests the field-aligned flow was probably characteristic of steady-state polar wind outflow of light ions, the flux of O^+ ions seen at EISCAT altitudes balancing the light ion outflow from the topside. This implies a sub-auroral location for Tromsø. [As shown in TITHERIDGE (1976) 'polar wind' flow is not confined to the region of open field lines—the most poleward closed flux tubes are so voluminous that they represent a sink as effective as the open ones.] The substorm caused enhanced precipitation and enhanced upward flow of thermal plasma along the Tromsø field line. This upward flow persisted for nearly 2 h and enhanced ion loss to the magnetosphere, in particular of O^+ ions, was possible in addition to any transient filling of the topside ionosphere in response to the precipitation enhancement.

Acknowledgements—The authors would like to thank the following members of the RAL EISCAT Section: D. M. WILLIS and A. P. VAN EYKEN for their support and scientific discussions and S. R. CROTHERS for the graphical presentations of the data. They are also most grateful to M. A. HAPGOOD, of the World Data Centre C1 for Solar-Terrestrial Physics (Rutherford Appleton Laboratory), for processing the ISEE-3 data.

The EISCAT Scientific Association is supported by the Centre National de la Recherche Scientifique of France, Suomen Akatemia of Finland, Max-Planck Gesellschaft of West Germany, Norges Almenvitenskapelige Forskninsgråd of Norway, Naturvetenskapliga Forskningsrådet of Sweden and the Science and Engineering Research Council of the United Kingdom. We acknowledge with thanks the assistance of the Director and staff of EISCAT.

REFERENCES

AKASOFU S.-I. 1981 *Space Sci. Rev.* **28**, 121.
AKASOFU S.-I., PERREAULT P. D., YASUHARA F. and MENG C.-I. 1973 *J. geophys. Res.* **78**, 7490.
BANKS P. M. and KOCKARTS G. 1973 *Aeronomy, Part B*, Academic Press.
BROMAGE B. J. I. 1984 *J. atmos. terr. Phys.* **46**, 577.
BURKE W. J., KELLEY M. C., SAGALYN R. C., SMIDDY M. and LAI S. T. 1979 *Geophys. Res. Lett.* **6**, 21.
FOSTER J. C., ST.MAURICE J.-P. and ABREU V. J. 1983 *J. geophys. Res.* **88**, 4885.
GUSSENHOVEN M. S., HARDY D. A. and BURKE W. J. 1981 *J. geophys. Res.* **86**, 768.
HARDY D. A., BURKE W. J., GUSSENHOVEN M. S., HEINEMANN N. and HOLEMAN E. 1981 *J. geophys. Res.* **86**, 9961.
HEELIS R. A. and HANSON W. B. 1980 *J. geophys. Res.* **85**, 1995.
HOFFMAN J. H. and DODSON W. H. 1980 *J. geophys. Res.* **85**, 626.
HOFFMAN J. H., DODSON W. H., LIPPINCOTT C. R. AND HAMMACK H. D. 1974 *J. geophys. Res.* **79**, 4246.
HORWITZ J. L. and AKASOFU S.-I. 1979 *J. geophys. Res.* **84**, 2567.
KAMIDE Y. and WINNINGHAM J. D. 1977 *J. geophys. Res.* **82**, 5573.
KIVELSON M. G. and SOUTHWOOD D. J. 1975 *J. geophys. Res.* **80**, 3528.
LOCKWOOD M. 1982 *Planet. Space Sci.* **30**, 595.
LOCKWOOD M. 1983 Private communication.
LOCKWOOD M. and TITHERIDGE J. E. 1981 *Geophys. Res. Lett.* **8**, 381.
MAEZAWA K. 1976 *J. geophys. Res.* **81**, 2289.
NYGREN T. 1977 *J. atmos. terr. Phys.* **34**, 733.
OLIVER W. L., HOLT J. M., WAND R. H. and EVANS J. V. 1983 *J. geophys. Res.* (In press).
REES D., FULLER-ROWELL T. J. and SMITH R. W. 1980 *Planet. Space Sci.* **28**, 919.
REIFF P. H. 1982 *J. geophys. Res.* **87**, 5976.
REIFF P. H., SPIRO R. W. and HILL T. W. 1981 *J. geophys. Res.* **86**, 7639.
RISHBETH H. 1977 *J. atmos. terr. Phys.* **39**, 111.
ROBLE R. G. and REES M. H. 1977 *Planet. Space Sci.* **25**, 991.
RUSSELL C. J. 1971 *Cosmic Electrodyn.* **2**, 184.
SCHLEGEL K. and ST.MAURICE J. P. 1981 *J. geophys. Res.* **86**, 1447.
SCHUNK R. W. and RAITT W. J. 1980 *J. geophys. Res.* **85**, 1255.
SOJKA J. J., SCHUNK R. W. and RAITT W. J. 1982 *J. geophys. Res.* **87**, 187.
STAMNES K. and REES M. H. 1983 *Geophys. Res. Lett.* **10**, 309.
TITHERIDGE J. E. 1976 *Planet. Space Sci.* **24**, 229.
WHITTEKER J. H. 1977 *Planet. Space Sci.* **25**, 773.